Effects of Vortex Separation on the Lift Distribution on Bodies of Elliptic Cross Section

LEON H. SCHINDEL*
U. S. Naval Ordnance Laboratory, White Oak, Md.

Vortex separation from slender bodies causes nonlinear increases of lift with angle of attack. A two-vortex representation of the separated flow is analyzed for bodies of elliptic cross section and arbitrary nose contour. The delta wing theory of Brown and Michael and the circular cone and cylinder solutions of Bryson are special cases of the more general geometry analyzed here. Comparisons with experiment show good agreement over a significant range of values of geometrical and flow parameters.

Nomenclature

A = reference (maximum) value of a
a = vertical semiaxis (in pitch plane) of elliptic cross section
B = reference (maximum) value of b
b = horizontal semiaxis (normal to pitch plane) of elliptic cross section
D = mean diameter of reference cross section $= 2(AB)^{1/2}$
F_f = force on feeding sheet
F_v = force on vortex
h = $\frac{1}{2}(a + b)$
K = constant determining rate of change of separation angle
k = $\frac{1}{2}(b^2 - a^2)^{1/2}$
l = body length
M = stream Mach number
N = normal force
U = freestream velocity
u = component of cross flow along x (real) axis
v = component of cross flow along y (imaginary) axis
w = local velocity due to cross flow about cylinder and vortices
w_1 = velocity at vortex location
x = real axis in Z plane
y = imaginary axis in Z plane
Z = cross-flow plane on circular body
z = distance along body axis
α = local body angle of attack
α_0 = average body angle of attack
β = angle from σ_0 to σ_1
Γ = vortex strength
δ = semivertex angle of cone $= \tan^{-1}(ab)^{1/2}/z$
ζ = point in cross-flow plane of elliptic body $= \xi + i\eta$
ζ_0 = location of separation point
ζ_1 = location of vortex
θ_0 = angular position of separation point
θ_∞ = equilibrium angle of separation
$\theta_{\infty CIR}$ = equilibrium angle of separation on body of revolution
λ = nondimensional vortex strength $= \Gamma/2\pi Ub \sin\alpha$
λ_{sep} = empirical constant fixing vortex strength at separation
μ = real axis in σ-plane
μ_0 = real coordinate of separation point in σ-plane
ν = imaginary axis in σ-plane
ν_0 = imaginary coordinate of separation point in σ-plane
ρ = freestream density
σ = transformed plane in elliptic coordinates $= \cosh^{-1}(\zeta/2k) = \mu + i\nu$
σ_0 = location of separation point in σ-plane
σ_1 = location of vortex in σ-plane
Φ = complex velocity potential $= \varphi + i\psi$
φ = velocity potential
ψ = stream function

Received November 21, 1968; revision received June 3, 1969. Most of the work reported here was completed while the author was at the Aerophysics Laboratory, Massachusetts Institute of Technology. Numerical computations were programmed by C. J. Borland and made use of the facilities of the Massachusetts Institute of Technology, Computation Center. Experimental contributions were made by E. G. Friberg and T. E. Chamberlain. The project was supported by the Naval Ordnance Systems Command.

* Chief, Aerodynamics Department. Member AIAA.

I. Introduction

THE lift on slender bodies at high angles of attack is strongly influenced by the separation of a pair of vortices from the lee side (see Fig. 1). As a result of this separation, the normal force becomes much larger at angles of attack above about 10° than would have been expected for a non-separated flow; the increase of normal force with angle of attack is strongly nonlinear; the center of pressure is moved aft by the separation. Furthermore, the separated vortices can significantly influence the forces on aft lifting surfaces or engine inlets.

H. J. Allen[1] proposed one of the first methods of calculating the nonlinear lift on bodies of revolution. He approximated the cross flow at each axial station by the corresponding steady flow about a two-dimensional cylinder. The nonlinear part of the force at each station was thus assumed to be equal to a local cross-flow drag, values for which were available

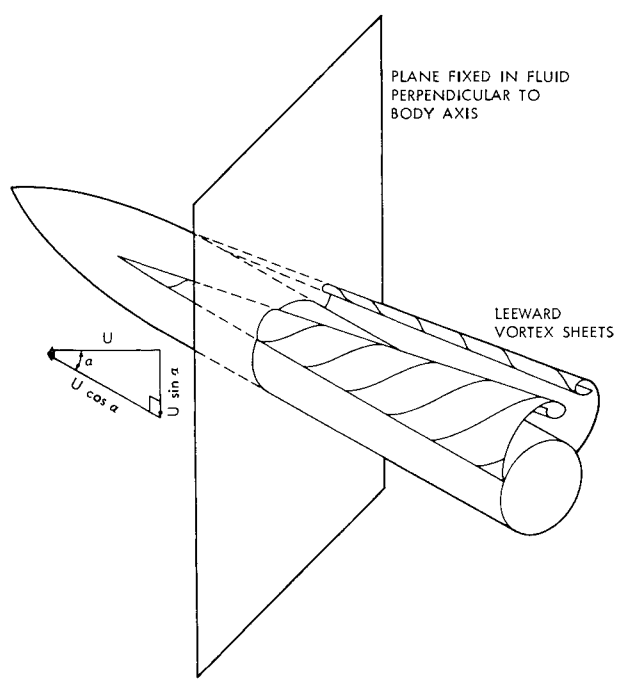

Fig. 1 Flow separation on a slender body at high angle of attack

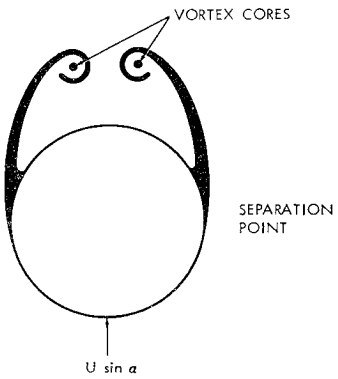

Fig. 2 Cross section of flow at a typical station along a circular body at angle of attack.

from two-dimensional experiments. A more appropriate analogy (as Allen noted) would identify the cross flow at different axial stations with the flow at corresponding times about a two-dimensional cylinder started from rest; the time coordinate being proportional to distance along the body. Using Schwabe's data[2] for the time-varying cross force (drag) on an impulsively started cylinder, Kelly[3] successfully correlated the nonlinear normal force and pitching moment on bodies of revolution on the basis of this analogy. The procedure was applied at supersonic speeds, to Mach numbers greater than three, as well as subsonically.

Hill[4] developed a separated vortex model from which he could calculate the cross-flow development on bodies of revolution, and thus was not dependent on Schwabe's experimental data. By introducing image vortices within the body, Bryson[5] was able to satisfy the boundary conditions on the surface, whereas Hill's solution only approximates the flow at the body surface. Bryson's solution, on the other hand, was restricted to circular cones and cylinders, whereas Hill's procedure could be used for circular bodies of more general nose shape.

In this paper, Bryson's two-vortex model will be extended to bodies of elliptic cross section and general contour. In the case of an ellipse of zero thickness, the body collapses into a flat plate; the analysis of the nonlinear lift on a delta wing by Brown and Michael[6] is thus a special case of the present theory.

In the next section, the physical characteristics of the flow with vortex separation will be described, along with the simplified approximation of this flow that is to be analyzed. The analysis is presented in Sec. III and compared with experiment in Sec. IV. Based on a number of experiments reported in Ref. 7, the theory appears to be valid over a range of Mach number, angle of attack, and body fineness ratio. The limitations are indicated near the end of the paper.

II. Representation of Flow with Vortex Separation

A. Separation and Roll-Up of Vortex Sheets

The primary features of the flow are illustrated in Fig. 1. The flow about the body separates as it tries to stream up around the sides against an adverse pressure gradient. The separated flow rolls up into a pair of concentrated vortices connected to the body by the feeding sheets indicated in the figure. A cross section of the flow at some axial station would look something like the illustration shown in Fig. 2. An actual flow pattern is shown in Fig. 3 where the vortices and their feeding sheets are made visible by the radiating grid technique described in Ref. 7. The body itself lies just below the illuminated portion of the flow and is not visible in the photograph.

The flow pattern is complicated by the presence of weak secondary vortices lying close to the body. Furthermore, at supersonic speeds, embedded shock waves may appear. These features, and other details of the flow are described in Refs. 8 and 9. On a very long body, the primary vortex pair may become unsymmetrical, and further aft on the body, one vortex would then break away from its feeding sheet. A new vortex would form close to the body. This unsymmetrical pattern, described and illustrated in Ref. 10, has been observed to shift suddenly from time to time. The phenomenon of vortex bursting has also been observed in the flow over delta wings and cones (Ref. 11).

In the present paper, an approximation of the separated flow pattern will be analyzed in which only the primary vortices are represented. This idealized flowfield, described in the following subsection, gives a reasonably good determination of the nonlinear lift forces on slender bodies. However, since the assumed model neglects important features of the actual flow, the theory becomes inadequate outside of certain ranges of geometric and flowfield parameters.

B. Two-Vortex Approximation

The flow, sketched in Fig. 1, is idealized by assuming that the shed vorticity has all rolled up into a pair of concentrated vortices connected to the body by straight feeding sheets of zero strength. This model is illustrated in Fig. 4. A cross section of the flow (taken normal to the body axis) is shown in Fig. 5.

An analysis of this model will produce the positions and strengths of the vortices as functions of distance along the body axis. In the theory, the separation angle θ_0 must be prescribed as a function of distance along the body. The normal force distribution can then be calculated from the body shape and the vortex development.

III. Analysis

A. Slender-Body Assumption

Assuming that the body is slender, the differential equation governing the flow in any cross section becomes a Laplace equation

$$(\partial^2\varphi/\partial x^2) + (\partial^2\varphi/\partial y^2) = 0 \qquad (1)$$

where $\varphi(x,y)$ is a velocity potential in the $(x\text{-}y)$ plane at any station at point z along the body axis. The application of the slender-body assumption to this problem is discussed in a little greater detail in Ref. 12.

B. Equations for Cross Flow

The Laplace equation corresponding to an incompressible two-dimensional flow must be solved at each cross section. The solutions will be derived first for the flow about a body of

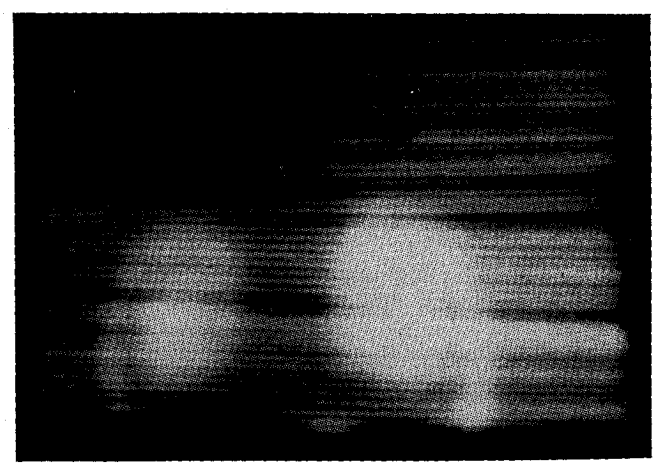

Fig. 3 Radiating grid photograph of a cross section of the flow on the lee side of an elliptic body at 20° angle of attack (α = 20°).

revolution, and then generalized by a conformal transformation to bodies of elliptic cross section.

For a circular cylinder in a vertical cross flow of velocity $v = U \sin\alpha$, the complex velocity potential (or potential function) is†

$$\Phi_c(Z) = -iv[Z - (h^2/Z)] \quad (2)$$

where $Z = x + iy$, h = radius of cylinder, and $\Phi = \varphi + i\psi$, $\psi(x,y)$ being the stream function.

A vortex of strength Γ at Z_1 (both Γ and Z_1 being functions of body station z) contributes the additional potential

$$\Phi_{\Gamma_1} = (-i\Gamma/2\pi) \ln(Z - Z_1) \quad (3)$$

To account for the separated vortex pair at Z_1 and $-\bar{Z}_1$, two solutions of this type are required. In addition, to preserve the boundary condition of no cross flow at the surface of the body, image vortices may be placed at the inverse points $h^2/\bar{Z}_1$ and $-h^2/Z_1$.

Finally, at points where the body radius is changing (near the nose for example), a source must be added to displace the stream by an amount equal to the local slope of the body contour.

$$\Phi_s = hU \cos\alpha_0(dh/dz) \ln(Z) \quad (4)$$

where $U \cos\alpha_0$ is the component of freestream velocity along the body axis.

The entire complex velocity potential representing the flow about an expanding (or contracting) circular cylinder with a pair of separated vortices is

$$\Phi = iv\left(Z - \frac{h^2}{Z}\right) - \frac{i\Gamma}{2\pi} \ln \frac{(Z - Z_1)[Z + (h^2/Z_1)]}{[Z - (h^2/\bar{Z}_1)](Z + \bar{Z}_1)} + hU \cos\alpha \frac{dh}{dz} \ln Z \quad (5)$$

The velocity at any point in the field can now be determined by differentiating the complex potential

$$\bar{w} = u - iv = d\Phi/dZ \quad (6)$$

where $w = u + iv$ = complex velocity, u = real (x) component of velocity, and v = imaginary (y) component of velocity.

The flow about a body of elliptic cross section is easily determined by applying the transformation

$$Z = \tfrac{1}{2}[\zeta + (\zeta^2 - 4k^2)^{1/2}] \quad (7)$$

where ζ = is a point in the cross-sectional plane of an elliptic body whose vertical dimension is $2a$ and whose width is $2b$

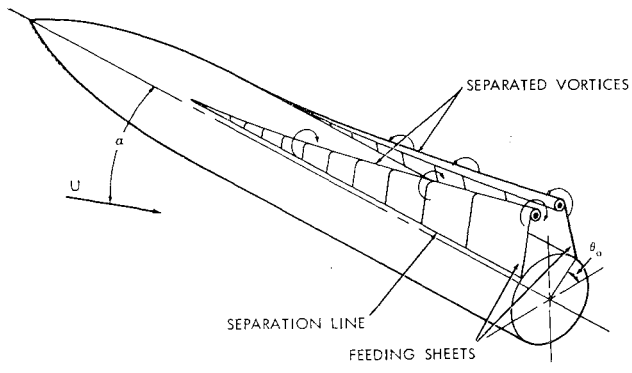

Fig. 4 Idealized model of the vortex separation on the lee side of a lifting body.

† The solutions given here may be found in any text on two-dimensional incompressible flow such as Milne-Thomson (Ref. 13).

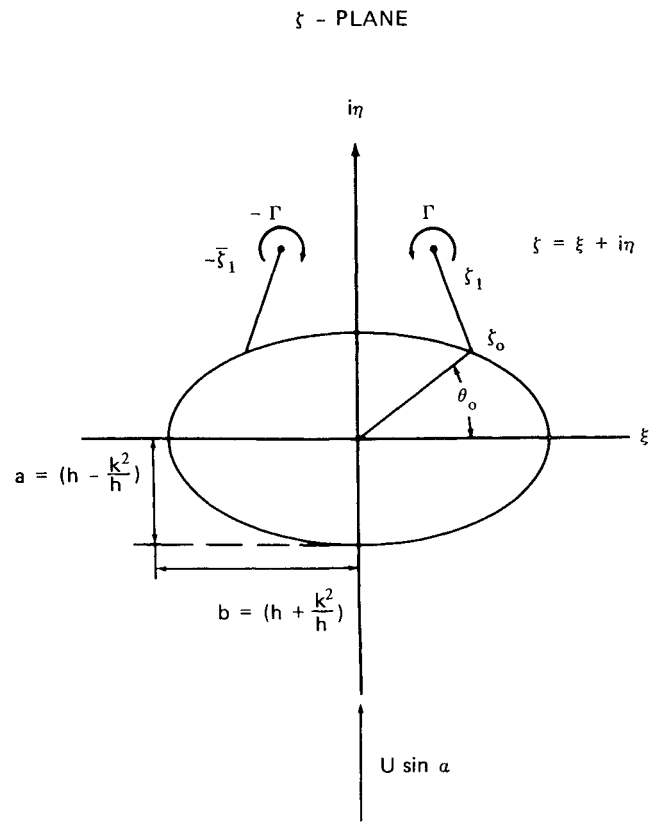

Fig. 5 Two-vortex model for the cross flow about an elliptic body.

(see Fig. 5), and $4k^2 = b^2 - a^2$. Note that only symmetric orientations (no yaw) are analyzed.

C. Force Balance and Separation Condition

The strengths and locations of the vortices are determined by requiring the force on each vortex to balance that on its feeding sheet, and by specifying that the separation points be stagnation points of the cross flow. These conditions, which are invoked also in Refs. 4, 5, and 6, among others, are consistent with the assumed two-vortex model. Other approximations are possible, however.

The vector force F_v, acting on the vortex at the point ζ_1 in the ζ plane is

$$F_v = \rho\Gamma[w_1 - U \cos\alpha_0(d\zeta_1/dz)] \quad (8)$$

where w_1 is the velocity at ζ_1 due to all elements of the flow except the vortex itself; thus,

$$\bar{w}_1 = \{d/d\zeta[\Phi + i\Gamma/2\pi \ln(\tfrac{1}{2}\zeta + \tfrac{1}{2}[\zeta^2 - 4k^2]^{1/2} - \tfrac{1}{2}\zeta_1 - \tfrac{1}{2}[\zeta_1^2 - 4k^2]^{1/2})]\}_{\zeta=\zeta_1} \quad (9)$$

The term containing $d\zeta_1/dz$ accounts for the velocity induced by the motion of the vortex.

The corresponding force on the feeding sheet is given by

$$F_f = \rho U \cos\alpha_0(d\Gamma/dz)(\zeta_1 - \zeta_0) = F_v \quad (10)$$

Although the feeding sheet is assumed to have zero strength, it must have a finite circulation since it is required to supply vorticity to the separated vortex at the rate $d\Gamma/dz$. Combining Eqs. (8) and (10) gives the force balance condition:

$$w_1 = U \cos\alpha_0 \left[\frac{d\zeta_1}{dz} + \frac{(\zeta_1 - \zeta_0)}{\Gamma} \frac{d\Gamma}{dz}\right] \quad (11)$$

The separation condition requires

$$w = 0 \text{ at } \zeta = \zeta_0 \quad (12)$$

Substitution for w from Eq. (6) results in the following equation relating the nondimensional vortex strength $\lambda = \Gamma/2\pi Ub \sin\alpha$ to its position:

$$\lambda = \frac{1}{2bk^2} \times \frac{[(h^2+k^2)([\zeta_0^2-4k^2]^{1/2}+[\bar{\zeta}_1^2-4k^2]^{1/2})-(h^2-k^2)(\zeta_0+\bar{\zeta}_1)]}{(h^2-k^2)(\zeta_1+\bar{\zeta}_1)-(h^2+k^2)[(\zeta_1^2-4k^2)^{1/2}+(\bar{\zeta}_1^2-4k^2)^{1/2}]} \times$$
$$[(h^2+k^2)([\zeta_0^2-4k^2]^{1/2}-[\zeta_1^2-4k^2]^{1/2})-(h^2-k^2)(\zeta_0-\zeta_1)] \quad (13)$$

The force balance provides an additional complex equation for vortex growth and trajectory

$$\left(\frac{1}{\lambda}\frac{d\lambda}{dz}+\frac{1}{b}\frac{db}{dz}+\frac{1}{\tan\alpha}\frac{d\alpha}{dz}\right)(\zeta_1-\zeta_0)+\frac{k^2-h^2}{h(\bar{\zeta}_1^2-4k^2)^{1/2}}\frac{db}{dz}+\frac{d\zeta_1}{dz}=$$
$$i\tan\alpha\left\{\frac{1}{2k^2}\left[k^2-h^2+\bar{\zeta}_1\frac{k^2+h^2}{(\bar{\zeta}_1^2-4k^2)^{1/2}}\right]-b\lambda\left[\frac{k^2-h^2+\bar{\zeta}_1[(h^2+k^2)/(\bar{\zeta}_1^2-4k^2)^{1/2}]}{(k^2-h^2)(\zeta_1+\bar{\zeta}_1)+(k^2+h^2)[(\bar{\zeta}_1^2-4k^2)^{1/2}+(\zeta_1^2-4k^2)^{1/2}]}\right]-\right.$$
$$\left.b\lambda\left[\frac{2k^2(k^2+h^2)}{(k^2-h^2)(\bar{\zeta}_1^2-4k^2)^{3/2}+\bar{\zeta}_1(k^2+h^2)(\bar{\zeta}_1^2-4k^2)}\right]\right\} \quad (14)$$

Here, the body is at some angle of attack α_0 but may be cambered slightly so that the local angle of attack (and hence the cross flow at each station) varies. The parameters h and k define the scale and eccentricity of the elliptical sections: $h = \frac{1}{2}(b+a)$ and $k^2 = (b^2-a^2)/4$. In transforming the source term, it has been assumed that b/a is constant over the entire body.

For a body of revolution, of radius h, $k^2 \to 0$ and the equations reduce to

$$h\lambda = (\zeta_1-\zeta_0)(\bar{\zeta}_1-\bar{\zeta}_0)(\zeta_1+\bar{\zeta}_0)(\bar{\zeta}_1+\zeta_0)/(\zeta_1\bar{\zeta}_1-h^2)(\zeta_1+\bar{\zeta}_1) \quad (15)$$

$$\left(\frac{1}{\lambda}\frac{d\lambda}{dz}+\frac{1}{h}\frac{dh}{dz}+\frac{1}{\tan\alpha}\frac{d\alpha}{dz}\right)(\zeta_1-\zeta_0)-\frac{h}{\bar{\zeta}_1}\frac{dh}{dz}+\frac{d\zeta_1}{dz}=i\tan\alpha\left[\frac{\bar{\zeta}_1^2+h^2}{\bar{\zeta}_1^2}+\right.$$
$$\left.h\lambda\left(\frac{1}{\bar{\zeta}_1+(h^2/\bar{\zeta}_1)}-\frac{1}{\bar{\zeta}_1-(h^2/\bar{\zeta}_1)}-\frac{1}{\zeta_1+\bar{\zeta}_1}\right)\right] \quad (16)$$

Equations (15) and (16) agree with Bryson's results for a circular cylinder when $dh/dz = d\alpha/dz = 0$. They reduce to his circular cone equations when, by conical similarity, $dh/dz = \tan\delta$; $d\alpha/dz = d\lambda/dz = 0$; and $d\zeta_1/dz = (\zeta_1/h)\tan\delta$ (δ being the cone semiapex angle). The case of the flat elliptic cone ($\alpha \to 0$) corresponds to the delta wing solution of Brown and Michael.

It is not difficult to integrate Eq. (14) numerically (on a computer), solving for vortex strength λ by Eq. (13) at each step of the computation. First, however, it is necessary to specify the separation line $\zeta_0(z)$, and to establish an initial condition.

D. Separation Line

The laminar separation lines are established empirically based on elliptic cone data reported in Ref. 14. The calculation of separation angle $\theta_0(z)$ proceeds in two steps. First, an equilibrium angle $\theta_\infty(z)$ is assigned to each axial station depending only on the local slope of the body surface.

$$\theta_\infty(z) = 90^\circ - \tan^{-1}[(b^2/a^2)\tan(90^\circ - \theta_{\infty CIR})] \quad (17)$$

where for laminar separation

$$\theta_{\infty CIR} = (13.12+\delta)[3.13-(0.116\alpha-1.16)^{1/2}]$$
$$10^\circ \leqq \alpha \leqq 40^\circ,\ 0^\circ \leqq \delta \leqq 15^\circ \quad (18)$$
$$\theta_{\infty CIR} = 3.13(13.12+\delta) \qquad 0^\circ \leqq \alpha \leqq 10^\circ,\ 0^\circ \leqq \delta \leqq 15^\circ$$

For turbulent separation, from comparison of predicted and measured nonlinear normal force on circular cones,

$$\theta_{\infty CIR} = 53^\circ \quad (19)$$

The angle δ (in degrees) is the semiapex angle of a cone tangent to the body at station z. For an elliptic cone δ is defined by

$$\tan\delta = (ab)^{1/2}/z \quad (20)$$

For a general body contour, the separation point does not immediately adjust to its equilibrium value θ_∞ whenever the local slope δ changes. A discontinuity in slope, such as on a cone-cylinder body, would not be expected to result in a discontinuous jump in separation angle. Instead, the separation angle is assumed to adjust to a change in body slope by exponentially approaching its equilibrium value in accordance with the following equation:

$$d\theta_0/dz = K(\tan\alpha/2a)(\theta_\infty - \theta_0) \quad (21)$$

This behavior of the motion of the separation point is analogous to the change of separation point with time observed during experiments on two-dimensional cylinders. The investigations reported in Ref. 15 indicate that a good value for K is 1.4.

The initial value for θ_0 is taken to be the value of θ_∞ at the point z; where the separation equations first have a solution. Criteria for determination of this point are described in the next section.

E. Initial Condition for Vortex Strength

The axial station at which separation begins is established by first finding, at a given angle of attack, the corresponding elliptic cone which would have an incipient vortex of infinitesimal strength lying just off its surface. Separation is assumed to begin at the station where the body surface is tangent to this elliptic cone.

The balance of forces on a vortex plus its feeding sheet results in the following special case of Eq. (14) for an elliptic cone.

$$2\zeta_1 - \zeta_0 - \frac{ab}{(\bar{\zeta}_1^2-4k^2)^{1/2}} = \frac{i(ab)^{1/2}\tan\alpha}{\tan\delta}\left\{-b\lambda\left[\frac{\bar{\zeta}_1[(h^2+k^2)/(\bar{\zeta}_1^2-4k^2)^{1/2}]-(h^2-k^2)}{(h^2+k^2)[(\zeta_1^2-4k^2)^{1/2}+(\bar{\zeta}_1^2-4k^2)^{1/2}]-(h^2-k^2)(\zeta_1+\bar{\zeta}_1)}+\right.\right.$$
$$\left.\left.\frac{2k^2(h^2+k^2)}{\bar{\zeta}_1(h^2+k^2)(\bar{\zeta}_1^2-4k^2)-(h^2-k^2)(\bar{\zeta}_1^2-4k^2)^{3/2}}\right]+\frac{1}{2k^2}\left[\bar{\zeta}_1\frac{h^2+k^2}{(\bar{\zeta}_1^2-4k^2)^{1/2}}-(h^2-k^2)\right]\right\} \quad (22)$$

Equation (13) for the vortex strength still holds.

Finding the angle of attack at which this equation first has a solution turns out to be simpler in elliptic coordinates (obtained by applying the transformation $\zeta = 2k\cosh\sigma$). Letting

$$\sigma_1 = \sigma_0 + \epsilon\exp(i\beta) \tag{23}$$

results in the following expression for departure angle β (in the σ-plane where $\sigma = \mu + i\nu$)

$$1/4\cos^2\beta = 1 - [4k^2\sin\nu_0/(ab)^{1/2}(a+b)]\tan\delta/\tan\alpha \tag{24}$$

Then, the cone equation first has a solution at the angle of attack corresponding to

$$\frac{\tan\alpha}{\tan\delta} = \frac{(b-a)[\sin^3\nu_0\cos^2\nu_0 + (3\sinh^2\mu_0 + 2\sin^2\nu_0 + \cos^2\nu_0)(\sinh^2\mu_0 + \sin^2\nu_0)]}{(ab)^{1/2}\sin\nu_0\cosh^2\mu_0} \tag{25}$$

For a circular cone, this condition reduces to

$$\tan\alpha/\tan\delta = 3/2\sin\nu_0 = 3/2\sin\theta_\infty \tag{26}$$

Unfortunately, at this axial station, where Eq. (25) is satisfied by the cone tangent to the body, the vortex strength is zero and its rate of growth is exponential. Hence, it would never develop. Therefore, an initial condition for integration of Eq. (14) is obtained by advancing along the body nose with tangent cones‡ until the vortex strength reaches an empirically established initial value λ_{sep}. Thus, the cone equation [Eq. (22)] is used, together with Eq. (13) to determine the vortex trajectory along the body until it comes to the station where $\lambda = \lambda_{sep}$. From this point on, the remainder of the trajectory is obtained by integrating Eq. (14).

The separation angle is obtained independently by the procedure described in the previous section. The calculation begins with $\theta_0 = \theta_\infty$ at the point where Eq. (25) is satisfied. At a discontinuity in slope, such as a cone-cylinder junction, the equilibrium angle $\theta\infty$ jumps in value but the actual separation angle θ_0 responds gradually in accordance with Eq. (21). Frequently, in fact, separation will begin at such a junction point on the body. The previously described procedures are then applied at this point just as though the slope were made continuous by an arc of vanishingly small radius.

To complete the specification of the initial condition, a method must be given for obtaining the value of λ_{sep}. The following empirical relations are recommended.

$$\lambda_{sep} = 0.150\frac{4ab}{(1+b)^2} \times \text{ if the boundary layer is laminar at separation} \tag{27}$$

$$\lambda_{sep} = 0.295\frac{4ab}{(a+b)^2} \times \text{ if the boundary layer is turbulent at separation}$$

These formulas give appropriate values for circular bodies ($a = b$) and taper off to zero for horizontal or vertical flat plates.

Whether the separation is laminar or turbulent will depend on surface roughness and freestream turbulence levels as well as the model size and shape. Assuming, however, that a transition Reynolds number is known, then the appropriate length seems to be an approximation of the local particle path as indicated in Fig. 6 for three typical stations. This criterion can only roughly distinguish between laminar and turbulent separation. In border-line cases, the actual flow geometry and accompanying pressure gradients will affect the location of transition.

‡ The equations for the vortex strength and position on a tangent cone have no solutions until a body station is reached where the apex angle is small enough to just satisfy the condition required by Eq. (25).

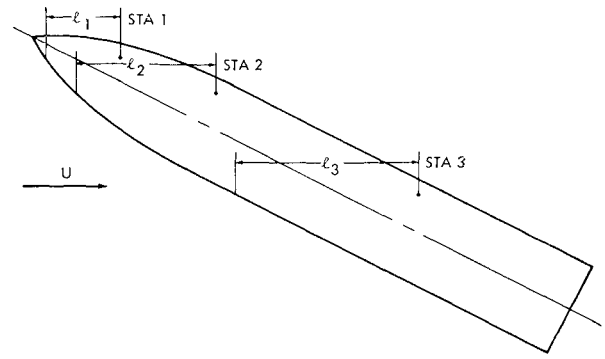

Fig. 6 Lengths for estimating boundary-layer transition.

F. Body Normal Force Distribution

Once vortex strengths and locations are known, the corresponding normal force increment at each body station may be found from a momentum balance. The procedure is described in Ref. 6, and applied to the body of elliptic cross section in Ref. 16. The resulting equation for the normal force accumulated up to station z is

$$N(z) = \rho U\cos\alpha_0\Gamma\,\text{R.P.}\{[(h^2+k^2)/k^2](\zeta_1^2 - 4k^2)^{1/2} - [(h^2-k^2)/k^2]\zeta_1\} + \pi\rho U^2(h + k^2/h)^2\cos\alpha_0\sin\alpha \tag{28}$$

The last term, which is independent of vortex strength, is the slender-body normal force.

For a body of revolution, $k^2 = 0$ and the expression becomes indeterminate. In the limit

$$N_{CIR}(z) = \rho U\cos\alpha_0\Gamma\,\text{R.P.}(2\zeta_1 - 2h^2/\zeta_1) + \pi\rho U^2h^2\cos\alpha_0\sin\alpha \tag{29}$$

IV. Comparison with Experiment

A. Numerical Calculations

The numerical process requires first solutions of the Eqs. (13 and 22) for vortex separation on tangent cones. These equations give vortex position ζ_1 and strength λ as functions of axial station. Because of their complexity, they are solved by iteration on an electronic computer. When the prescribed strength λ_{sep} has been achieved, the differential equation for vortex position (Eq. 14) is integrated by incrementing numerically from the previous step using the old values of λ at each increment. The term in $d\lambda/dz$ is entered in terms of the vortex position by analytically differentiating Eq. (13). When new values have been obtained for the vortex location, its strength can be determined from Eq. (13).

Calculations have been carried out for a number of bodies of elliptic cross section with various nose shapes and body fineness ratios. A computer program and results of the calculations are given in Ref. 7.

B. Comparison with Experiment

Subsonic wind-tunnel tests on families of elliptic bodies are reported in Ref. 7. Separation lines were measured from observations by the China-clay and paint-drop techniques; vortex paths were determined from tuft-grid studies; and forces and moments were measured by a strain-gage balance.

Only symmetric orientations were investigated (no yaw or roll angle); however, both laminar and turbulent cases were included. Some of the force and moment data are shown in Figs. 7 and 8 along with the calculated values. The body, in each case had a fineness ratio of 10 [based on a mean diameter defined by $D = 2(AB)^{1/2}$ (A and B are the semiaxes of the elliptic cross sections on the cylindrical portion of the body)]. Each body nose had an ogival contour three-calibers long. That is, the widest plan view of the nose was a tangent ogive.

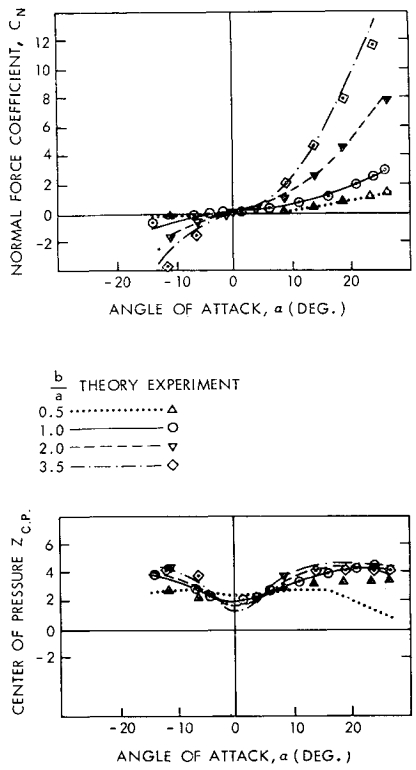

Fig. 7 Normal force and center of pressure on bodies of elliptic cross section with laminar separation.

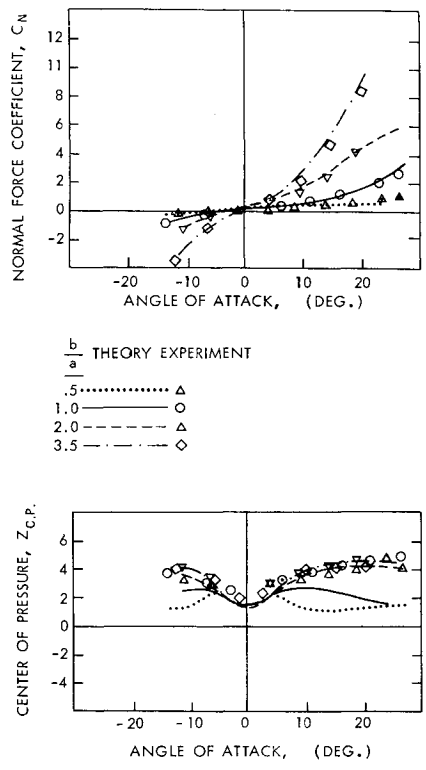

Fig. 8 Normal force and center of pressure on bodies of elliptic cross section with turbulent separation.

The theory predicts the force data quite well, particularly in the laminar case.§ At high angles of attack, the theory breaks down when the symmetric vortex pattern apparently becomes unstable (see Ref. 5 or 7). The tendency of the theory to underestimate the vortex-induced force toward the rear of the body is exaggerated in the center-of-pressure plots which, because of the effect of the large moment arm, are more sensitive to the reduced forces predicted for the after part of the body.

The measured vortex trajectories were generally in agreement with predictions. The separation lines, however, were not. Differences between measured and predicted separation angles occasionally exceeded 30°. These measurements also contradicted the data of Ref. 14 on which the present separation line formulas are based. It is possible that the hydrogen bubble method used in Ref. 14 indicates a separation line toward the outer edge of the boundary layer while the surface-type measurements show a separation line at the body end of the boundary layer. The success of the force theory would imply that the correlation used here is satisfactory for that purpose.

C. Limitations of the Theory

The slender body assumption implies $(M^2 - 1)^{1/2}(B/l) \ll 1$ where in this case B designates the body's widest dimension. The tests described in Ref. 7 were all at relatively low subsonic speed; but the theory is still successful by comparison with Kelly's data at Mach numbers up to 3.

From the full range of subsonic tests, the following limitations have been determined empirically: angle of attack or body length limit:

$$\frac{l}{A}\tan\alpha < \begin{matrix} 10 \text{ laminar} \\ 8 \text{ turbulent} \end{matrix}$$

At the limits, the lift prediction is good, but the theory for center of pressure has degraded somewhat.

§ The analysis took into account the fact that the flow became turbulent over aft parts of the bodies.

For delta wings, the theory predicts too great a nonlinear force, as may be seen in Refs. 6 and 17. This discrepancy has been charged to the nature of the two-vortex approximation. For delta wings, the nonlinear lift is not a large part of the total unless the aspect ratio is very small hence the error in total lift is not too serious. The theory can be usefully applied, then, to wings of $AR > 0.25$ and to general bodies of sufficient thickness that $l/A < 35$.

Pressure distributions are poorly predicted by the theory, principally because the vorticity in the feeding sheets has been neglected. More complicated models, such as those of Refs. 17 and 18 in which the vortex sheet is represented, seem to give reasonable pressure distributions.

References

[1] Allen, H. J., "Estimation of the Forces and Moments on Inclined Bodies of Revolution of High Fineness Ratio," RM A9I26, 1949, NACA.

[2] Schwabe, M., "Über Drukermittlung in der Nichstationären Ebenen Strömung," *Ingenieur-Archiv*, Bd. VI, No. 1, 1935; translated as TM 1039, 1943, NACA.

[3] Kelly, H. R., "The Estimation of Normal Force and Pitching Moment Coefficients for Blunt-Based Bodies of Revolution at Large Angles of Attack," Rept. TM 998, 1953, Naval Ordnance Test Station; also *Journal of the Aeronautical Sciences*, Vol. 21, No. 8, Aug. 1954.

[4] Hill, J. A. F., "A Nonlinear Theory of the Lift on Slender Bodies of Revolution," *Proceedings of the U. S. Navy Symposium on Aeroballistics*, NAVORD Report 5338, Oct. 1954.

[5] Bryson, A. E., Jr., "Symmetric Vortex Separation on Circular Cylinders and Cones," *Journal of Applied Mechanics*, Vol. 26, No. 4, Dec. 1959.

[6] Brown, C. E. and Michael, W. H., Jr., "On Slender Delta Wings with Leading Edge Separation," TN 3430, April 1955, NACA.

[7] Schindel, L. H. and Chamberlain, T. E., "Vortex Separation on Slender Bodies of Elliptic Cross Section," TR 138, Aug. 1967, M.I.T. Aerophysics Lab.

[8] Rainbird, W. J., "Turbulent Boundary-Layer Growth and

Separation on a Yawed 12½° Cone at Mach Numbers 1.8 and 4.25," AIAA Paper 68-98, New York, 1968; also *AIAA Journal*, Vol. 6, No. 12, Dec. 1968, pp. 2410–2416.

[9] Rodgers, E. J., "Real Flow over a Body of Revolution at Angle of Attack," Ph.D. thesis, 1963, Pennsylvania State Univ.

[10] Maltby, R. L. and Peckham, D. H., "Low Speed Flow Studies of the Vortex Patterns Above Inclined Bodies Using a New Smoke Technique," TN Aero 2482, 1956, Royal Aircraft Establishment.

[11] Benjamin, T. B., "Theory of the Vortex Breakdown Phenomenon," *Journal of Fluid Mechanics*, Vol. 14, Pt. 4, 1962.

[12] Schindel, L. H., "Separated Flow about Lifting Bodies," TR 80, Sept. 1963, M.I.T. Aerophysics Lab.

[13] Milne-Thomson, L. M., *Theoretical Hydrodynamics*, 4th ed., Macmillan, New York, 1960.

[14] Friberg, E. G., "Measurement of Vortex Separation, Part II: Three-Dimensional Circular and Elliptic Bodies," TR 115, Aug. 1965, M.I.T. Aerophysics Lab.

[15] Friberg, E. G., "Measurements of Vortex Separation, Part I: Two-Dimensional Circular and Elliptic Bodies," TR 114, July 1965, M.I.T. Aerophysics Lab.

[16] Schindel, L. H., "Effect of Vortex Separation on Lifting Bodies of Elliptic Cross Section," TR 118, Sept. 1965, M.I.T. Aerophysics Lab.

[17] Smith, J. H. B., "Improved Calculations of Leading-Edge Separation from Slender Delta Wings," TR 66070, March 1966, Royal Aircraft Establishment.

[18] Mangler, K. W. and Smith, J. H. B., "Calculation of the Flow Past Slender Delta Wings with Leading-Edge Separation," TN AERO 2593, May 1957, Royal Aircraft Establishment; also *Proceedings of the Royal Society (London), Ser. A*, Vol. 251, 1959, pp. 200–217.

NOV.-DEC. 1969 J. AIRCRAFT VOL. 6, NO. 6

Propagation of Error in the Calculation of Airplane Thrust and Drag

EVERETT W. DUNLAP*
Air Force Flight Test Center, Calif.

Knowledge of an airplane's drag polar is needed to establish the performance characteristics of the airplane. In-flight measurements are frequently made during the course of test programs to define drag polars. Inaccuracies in the measured variables can contribute to significant uncertainties in computed lift and drag coefficients. To gain an appreciation of the magnitude of these uncertainties, equations have been derived for an aircraft powered by a nonafterburning turbojet engine which express the inaccuracies in lift and drag coefficients in terms of inaccuracies in measured variables. As a by-product, the variables that are the source of the larger inaccuracies in the drag polar can be found and the need for improved instrumentation identified. Sample calculations were made using data from the Air Force performance tests on the A-37A, and inaccuracies in its drag polar, as well as in the intermediate answers (gross thrust, inlet momentum, and drag), are shown graphically. These calculations indicate that the most critical measurements are of turbine discharge pressure and vane alignment (to orient axes of accelerometers used to compute excess thrust); degradation of computed drag from errors in these variables is most pronounced at high lift coefficients.

Nomenclature

A_8 = nozzle area, ft²
C_D = drag coefficient, dimensionless
C_g = nozzle coefficient, dimensionless
C_L = lift coefficient, dimensionless
D = drag, lb
F_e = inlet momentum (ram drag), lb
F_{ex} = excess thrust, lb
F_g = gross thrust, lb
H = geopotential altitude, ft
$I(\ )$ = interval estimate of ( )
K_1 = 6.87535×10^{-6}, 1/geopotential ft
K_2 = 5.2561
K_3 = 17058.8 psf
K_4 = 0.43034 ft²/lb
K_5 = 661.48 knots
K_α = percentage point
M = Mach number, dimensionless
n_x = load factor along wind x-axis, dimensionless
n_z = load factor along wind z-axis, dimensionless
P_a = ambient pressure, in. Hg
P_{t_8} = turbine discharge pressure, in. Hg
S = wing area, ft²
T = ambient temperature, °K
V_c = calibrated airspeed, knots
V_t = true airspeed, knots
ΔV_c = compressibility correction $V_c = V_c + \Delta V_c$, knots
w_a = airflow, lb/sec
W = airplane gross weight, lb
ϵ = misalignment angle, rad
ρ_{sl} = air density at sea level, slugs/ft³
σ = standard deviation, air density ratio
σ^2 = variance

Superscript

* = nominal value

Received October 21, 1968; revision received April 21, 1969.
* Chief, Aircraft Research Section.

Introduction

Equations are derived for an aircraft powered by a nonafterburning turbojet engine which show how inaccuracies in variables measured in flight are reflected in an aircraft's performance parameters. With these equations the sensitivity of performance parameters to measured variables can be found. As an example, net thrust is a function of altitude, nozzle discharge pressure, nozzle area, nozzle coefficient, engine airflow, and calibrated airspeed. The sensitivity of net thrust to each of the independent variables can be found. With a knowledge of the inaccuracies of in-flight measurements, the corresponding errors in net thrust can be computed.